Superfluidity, Bose-Einstein condensation, and structure in one-dimensional Luttinger liquids

L. Vranješ Markić, H. Vrcan, Z. Zuhrianda, and H. R. Glyde

Phys. Rev. B **97**, 014513 — Published 19 January 2018

DOI: 10.1103/PhysRevB.97.014513

Superfluidity, BEC and structure in 1D Luttinger Liquids

L. Vranješ Markić,[1] H. Vrcan,[1] Z. Zuhrianda,[2] and H. R. Glyde[2]

[1] *Faculty of Science, University of Split, HR-21000 Split, Croatia, EU*

[2] *Department of Physics and Astronomy, University of Delaware, Newark, Delaware 19716-2593, USA*

(Dated: December 31, 2017)

We report diffusion Monte Carlo (DMC) and path integral Monte Carlo (PIMC) calculations of the properties of a 1D Bose quantum fluid. The equation of state, the superfluid fraction, ρ_S/ρ_0, the one-body density matrix, $n(x)$, the pair distribution function, $g(x)$, and the static structure factor, $S(q)$, are evaluated. The aim is to test Luttinger Liquid (LL) predictions for 1D fluids over a wide range of fluid density and LL parameter K. The 1D Bose fluid examined is a single chain of ^{4}He atoms confined to a line in the center of a narrow nanopore. The atoms cannot exchange positions in the nanopore, the criterion for 1D. The fluid density is varied from the spinodal density where the 1D liquid is unstable to droplet formation to the density of bulk liquid ^{4}He. In this range, K varies from $K > 2$ at low density, where a robust superfluid is predicted, to $K < 0.5$, where fragile 1D superflow and solid-like peaks in $S(q)$ are predicted. For uniform pore walls, the ρ_S/ρ_0 scales as predicted by LL theory. The $n(x)$ and $g(x)$ show long range oscillations and decay with x as predicted by LL theory. The amplitude of the oscillations is large at high density (small K) and small at low density (large K). The K values obtained from different properties agree well verifying the internal structure of LL theory. In the presence of disorder, the ρ_S/ρ_0 does not scale as predicted by LL theory. A single v_J parameter in the LL theory that recovers LL scaling was not found. The one body density matrix (OBDM) in disorder is well predicted by LL theory. The "dynamical" superfluid fraction, ρ_S^D/ρ_0, is determined. The physics of the deviation from LL theory in disorder and the "dynamical" ρ_S^D/ρ_0 are discussed.

I. INTRODUCTION

Dimensions play a key role in determining exotic phenomena such as Bose-Einstein condensation (BEC) and superfluidity. In 3D, BEC begins at a well-defined finite temperature[1–4] T_{BEC}. Below T_{BEC}, a finite fraction of the Bosons occupy one single particle state and the one-body density matrix (OBDM) develops a long-range tail[4–6]. In bulk, uniform systems, the tail is flat and extends to infinity. Superfluidity (and superconductivity) can be formulated[7] as arising from the coherent field established by the macroscopically occupied state. T_c for superflow equals T_{BEC}. Below T_c, the superfluid fraction, ρ_S/ρ, increases smoothly with decreasing temperature, from zero at T_c to unity at 0 K.

In 2D systems at low temperature, the OBDM develops a tail that decays algebraically with distance. In 2D liquid ^{4}He the algebraic tail can extend[6] to over 100 Å, but is not macroscopic. A T_{BEC} in 2D can be defined as the temperature at which the OBDM first develops this algebraic tail. Superfluidity in 2D is generally formulated[8,9] independently of BEC. There is an abrupt jump in ρ_S/ρ from zero to a finite fraction[9] at T_c, in contrast to 3D. T_c can also be identified[8] from the OBDM as the temperature at which the exponent that describes the algebraic tail reaches a specific value.

In 1D spinless Bose and Fermi fluids, low energy phenomena such as superflow and BEC is expected to follow the predictions of Luttinger Liquid (LL) theory[10]. The OBDM is predicted to show a decaying algebraic tail at low temperature that has oscillations which extend to large distances reflecting the atomic order in 1D. The pair distribution function (PDF) has similar long-range oscillations. These oscillations are uniquely characteristic of 1D and are not seen in the OBDM or PDF in 2D or 3D fluids. Superfluidity in 1D is really only a finite size effect. There is no T_c. The ρ_S/ρ_0 has a characteristic 1D shape and scales as LT, the product of the temperature, T, and length, L, of the 1D system.

There has been an extensive search for 1D quantum fluids. ^{4}He or other Bosons confined in small diameter nanopores may show 1D behavior[11–17]. Most of the ^{4}He in the nanopores is deposited in layers (solid and liquid) on and near the pore walls.[11–16,18,19] These layers have properties characteristic of 2D or 3D. Those atoms confined to the center or core of the nanopore could be a 1D system.[20–22] ^{4}He confined to a dislocation in solid helium is also predominantly a 1D system[23]. ^{4}He and other atoms confined in and on carbon nanopore bundles can show 1D character.[24]

Cold atoms in highly asymmetric optical lattices can be tightly restricted in two dimensions but highly extended in the third dimension[25,26]. While atomic displacements in all directions are possible, exchange and tunneling between lattice sites are predominantly along the extended 1D. The central goal of this exciting field is to explore transitions from superfluidity to Mott-insulator[27,28] or Bose Glass[29–32] states, and to determine critical momentum[33] and phase slips[34]in 1D. Superconductivity in 1D is also anticipated in nanowires[35]. Specifically, the role of phase slips in loss of superflow in nanowires has been extensively investigated[36]. The theory of 1D systems has been equally extensively developed[37–42] .

The goal of the present paper is to display the properties of a genuine 1D Bose quantum fluid. It is particularly

to test whether the properties are well predicted by LL theory. We consider liquid ^{4}He confined to a line in a narrow nanopore of radius $R = 3$ Å. The nanopore wall represents the amorphous solid layers of ^{4}He (1.5 layers) on the interior of the nanopore as well as the nanopore[43]. We present DMC calculations of the equation of state (EOS), the pair distribution function (PDF), $g(x)$, and the static structure factor, $S(q)$, and PIMC calculations of the superfluid fraction, ρ_S/ρ_0, and the one-body density matrix (OBDM), $n(x)$, of the confined liquid. The aim is to verify LL predictions as a function of the 1D density and the value of the LL parameter K which is a sensitive function of density. It is also to display clearly the properties of 1D fluids as a function of the LL parameter, K. With a clear picture of a 1D fluid, we can more readily identify whether experimentally investigated systems show 1D properties rather than 2D or 3D character. We also evaluate the "dynamical" superfluid fraction defined in Refs. 44 and 45.

Liquid ^{4}He at reduced dimension has been investigated recently using PIMC methods. Del Maestro and Affleck[46] explored pure 1D helium, a line of N Bosons in a length L, in the grand canonical ensemble. They showed that the distribution of N about its equilibrium value, N_0, and the distribution of winding numbers, W, were Gaussian and well predicted by LL theory with corrections at higher energy. Del Maestro et al.[20,21] and Kulchytskyy et al.[22] explored ^{4}He confined in nanopores. They found that most of the ^{4}He is deposited on and near the pore walls, first as solid and then liquid layers. However, at some pore radii, a fraction of the liquid is confined to a line at the center of the pore. This fraction may be considered a 1D liquid. The total ρ_S/ρ of the ^{4}He appeared to fulfill LL predictions although this was not well-established.[22]. Vranješ Markić and Glyde[43] considered liquid ^{4}He in a model nanopore chosen to represent both the nanopore and the solid ^{4}He layers on the pore walls. In this way, only the liquid in the nanopore need be simulated using PIMC. The density was set at the bulk liquid density. For liquid pore radii $R \geq 4$ Å, most of the ^{4}He lay in liquid layers close to the pore walls with a small fraction in a 1D core at the center of the pore. At $R \geq 4$ Å the ρ_S/ρ and OBDM scaled as expected for 2D and or 3D liquids.[43,47]. However for $R = 3$ Å all of the helium was found to lie on a line at the center of the pore. The ρ_S/ρ_0 and OBDM of the 1D line followed the LL predictions.

Liquid parahydrogen (p-H_2) has long been investigated as a possible superfluid. As for liquid ^{4}He, the search includes p-H_2 at reduced dimensions such as pure 2D p-H_2[48] and pure 1D p-H_2[48,49], and p-H_2 in carbon nanopores[24,49,50] and p-H_2 in a variety of other nanopores[51]. The similarity of 1D ^{4}He and p-H_2 is discussed in section IV.

In this context our goal is to calculate the properties of 1D liquid ^{4}He in a narrow nanopore of liquid pore radius $R = 3$ Å in which (1) there is only 1D liquid ^{4}He (no other 2D or 3D ^{4}He in layers), (2) the density can be varied and (3) disorder can be added. Over the range of 1D densities considered, the LL parameter $K = (v_J/v_N)^{1/2}$ varies from $K < 0.5$ (solid-like correlations) to $K > 2$ (a robust superfluid). The aim is to test LL theory.[10,37–39]

II. LUTTINGER LIQUID PREDICTIONS

In this section we outline the predictions made from LL theory. Haldane[10] and others[37–39,46] consider a 1D line of N bosons of average density $\rho_0 = N_0/L$ with periodic boundary conditions over a length L. The field operator, $\Psi_B(x)$, in the general Hamiltonian H is expressed as a magnitude and a phase, $\phi(x)$, $\Psi_B^\dagger(x) = \rho(x)^{1/2}e^{i\phi(x)}$. For low energy, long wavelength fluctuations in the density $\rho(x)$, Haldane[10] shows that H may be simplified to,

$$\begin{aligned} H_{LL} &= \frac{\hbar}{2\pi}\int dx[v_J(\nabla\phi)^2 + v_N(\nabla\theta - \pi\rho_0)^2] \\ &= \hbar\left\{\sum_{q\neq 0}\omega_q b_q^\dagger b_q + \left(\frac{\pi}{2L}\right)\left[v_J J^2 + v_N(N-N_0)^2\right]\right\}. \end{aligned} \tag{1}$$

H_{LL} describes an effective harmonic fluid. The term $\frac{\hbar}{2\pi}v_J(\nabla\phi)^2$ represents the kinetic energy density. The density is $\rho(x) = \rho_0 + \Pi(x)$ where $\Pi(x)$ is a small and long wavelength change in $\rho(x)$ and $\nabla\theta \equiv \pi[\rho_0 + \Pi(x)]$. The term $\frac{\hbar}{2\pi}v_N(\nabla\theta - \pi\rho_0)^2 = \frac{\hbar}{2\pi}v_N\Pi(x)^2$ represents the potential energy density of the density fluctuations. The ω_q are the frequencies of the density modes. Since $q = 2\pi/\lambda$ is small, $\omega_q = v_S q$ where v_S is the sound velocity. The index J denotes the number of phase twists in ϕ over the length L, $\phi(L) - \phi(0) = 2\pi J$, and $(N - N_0)$ is the deviation of N from the average $N_0 = \rho_0 L$. We consider a canonical ensemble in which N is fixed at $N = N_0$.

For a Galilean invariant, 1D LL $\hbar v_J^0 = \pi(\hbar^2/m)\rho_0$ and $\hbar v_N = (\pi\rho_0^2\kappa)^{-1}$ where κ is the 1D compressibility. At $T = 0$ K and expressing $V = AL$, the 1D compressibility is $\kappa^{-1} = A\kappa_T^{-1}$ where $\kappa_T^{-1} = -V(\partial p/\partial V)_T$ is the 3D compressibility. In terms of the 1D pressure $P = Ap$,

$$\kappa^{-1} = \rho_0\frac{\partial P}{\partial\rho_0}, \tag{2}$$

where $P = \rho_0^2\partial e/\partial\rho_0$ and $e = E/N$. Since $K = (v_J^0/v_N)^{1/2} = [\pi^2(\frac{\hbar^2}{m})\rho_0^3\kappa]^{1/2}$, large K corresponds to large κ, e.g. a gas like fluid. For $K > 2$ and $K > 3/2$ a superfluid robust to a periodic external potential and to disorder, respectively, is predicted[52]. Small K corresponds to small κ, e.g. a solid-like fluid at high density where superflow is fragile.

The sound velocity of the 1D LL density modes, given by the usual expression $v_S^2 = (m\rho_0\kappa)^{-1}$, can be written as $v_S = (v_J^0 v_N)^{1/2}$. The parameter K is often expressed as $K = v_J^0/v_S$ and $K = v_S/v_N$. The physics of 1D systems has been extensively reformulated and reviewed.[37–39]

From H_{LL}, Haldane and others make predictions that we denote LL predictions. For the pair distribution function (PDF), $g(x)$, $[\langle\rho(x)\rho(0)\rangle = \rho_0^2 g(x)]$, and the OBDM, $n(x)$, at long lengths $x \gg a = \rho_0^{-1}$ and $T = 0$ K, and the superfluid fraction, ρ_S/ρ_0, these are,[10,46]

$$g(x) = \frac{1}{\rho_0^2}\langle\rho(x)\rho(0)\rangle = \left[1 - 2K(2\pi\rho_0 x)^{-2} + \sum_{n=1}^{\infty}(\rho_0 x)^{-2Kn^2} A_n \cos(2\pi n\rho_0 x)\right] \tag{3}$$

$$n(x) = \langle\Psi_B(x)\Psi_B^\dagger(0)\rangle = \frac{\rho_0}{(\rho_0 x)^{1/2K}}\sum_{n=0}^{\infty}(\rho_0 x)^{-2Kn^2} B_n \cos(2\pi n\rho_0 x) \tag{4}$$

and

$$\frac{\rho_S}{\rho_0} = \left(\frac{TL}{\sigma\rho_0}\right)\langle W^2\rangle = \alpha_0\langle W^2\rangle \tag{5}$$

$$= \alpha_0 \sum_W W^2 e^{-\frac{1}{2}\alpha W^2} / \sum_W e^{-\frac{1}{2}\alpha W^2} \tag{6}$$

$$= \left(\frac{\alpha_0}{4}\right)\frac{|\Theta_3''(0, e^{-\alpha/2})|}{\Theta_3(0, e^{-\alpha/2})} \tag{7}$$

where $\alpha_0 \equiv (TL/\sigma\rho_0)$, $\sigma = \hbar^2/k_B m = 12.1193$ K Å^2, W is the winding number, $\Theta_3(z,q)$ is the Theta function, $\Theta_3''(z,q) = d^2\Theta_3(z,q)/dz^2$ and

$$\alpha = \left(\frac{\pi k_B TL}{\hbar v_J}\right) = \alpha_0(\frac{v_J}{v_J^0})^{-1}. \tag{8}$$

The expressions for $g(x)$ and $n(x)$ are Eqs. (3) and (4), respectively, of Haldane[10]. The coefficients A_n and B_n are not known. Our goal is to check how well the LL predictions for $g(x)$ and $n(x)$ fit our calculated $g(x)$ and $n(x)$ treating the LL parameter $K = (v_J/v_N)^{1/2}$ (and A_1 and B_1) as free fitting parameters.

Eq. (5) for ρ_S/ρ_0 is the general expression for the "thermodynamic" superfluid fraction ρ_S/ρ_0 in 1D in terms of the winding number W.[4,6,53] We calculate $\langle W^2\rangle$ using PIMC and evaluate ρ_S/ρ_0 from Eq. (5). DelMaestro and Affleck[46] have shown that the probability of observing a winding number W in a 1D LL is Gaussian,

$$P(W) \propto e^{-\frac{1}{2}\alpha W^2}, \tag{9}$$

with coefficient α given by Eq. (8). Eqs. (6) and (7) are the LL predictions for ρ_S/ρ_0 with $W = 0, \pm1, \pm2, ...$

To test LL predictions we fit Eq. (6) with $\hbar v_J$ treated as a free fitting parameter to the PIMC ρ_S/ρ_0 calculated from Eq. (5). For a Galilean invariant LL (no disorder or periodic external potential), $\hbar v_J \to \hbar v_J^0 = \pi(\hbar^2/m)\rho_0$, $(v_J/v_J^0 = 1)$, and $\alpha \to \alpha_0$. For a Galilean invariant LL, $v_J^0 = v_F$ where, v_F, is the Fermi velocity of a Fermi liquid at the same linear density, ρ_0. In a uniform 1D fluid, if it is a LL, we expect a good fit of Eq. (6) to the PIMC ρ_S/ρ_0 (low χ^2) with $v_J/v_J^0 = 1$. For a 1D LL in disorder we anticipate a good fit of Eq. (6) with a constant v_J but v_J may differ from v_J^0. For constant v_J, the LL ρ_S/ρ_0 still scales as the product LT rather than separately on L or T. In 1D ρ_S/ρ_0 is a finite size effect, there is no T_C and $\rho_S/\rho_0 \to 0$ as $L \to \infty$.

LL theory also predicts that the static structure factor, $S(q)$, will develop a peak at the first "reciprocal lattice" vector $q = 2\pi/a$ at high density ρ_0. The peak signals that the liquid at high density displays solid-like features. The LL parameter K can be obtained from the low q limit of $S(q)$,

$$K = 2\pi\rho_0 \lim_{q\to 0}\frac{S(q)}{q}. \tag{10}$$

Eq. (10) follows from the general relation between the sound velocity v_S and $S(q)$ valid in all dimensions, $\lim_{q\to 0} S(q) = \hbar q/2mv_S$ and the 1D (uniform) LL relation, $K = v_J^0/v_S$. The LL parameter may be calculated from: (a) the equation of state $e(\rho_0) = E(\rho_0)/N$ using Eq. (2), (b) from fits of the LL expression Eq. (3) to the calculated $g(x)$ and from the $q \to 0$ limit of $S(q)$, Eq. (10), and (c) from fits of the LL expression Eq. (4) to $n(x)$. If the predictions of LL theory are internally consistent, the K values obtained from these three routes should agree.

The equation of state $E(\rho_0)$ at $T = 0$ K was calculated using DMC methods as were $g(x)$, and $S(q)$ using the expressions,

$$g(x) = \frac{1}{\rho_0 N}\sum_{l\neq l'}^{N}\langle\delta(x - |x_l - x_l'|)\rangle, \tag{11}$$

and,

$$S(q) = \frac{1}{N}\langle\sum_{l,l'}^{N} e^{-iq\cdot[x_l - x_l']}\rangle. \tag{12}$$

The OBDM, $n(x)$, and the MC winding number $\langle W^2\rangle$ at finite temperature were calculated using the worm algorithm PIMC and standard methods[6]. To restate, we used the canonical ensemble version of the worm algorithm PIMC code in which N is fixed at $N = N_0$; $\rho_0 = N/L = N_0/L$.

To close this section, we note that a "dynamical" superfluid fraction, ρ_S^D, has been introduced.[45,54] This is in addition to the "thermodynamic" $\rho_S/\rho_0 =$

$\partial(F_v/N)/\partial(\frac{1}{2}mv^2) = \alpha_0\langle W^2\rangle$ defined above that we evaluate using PIMC. The "thermodynamic" ρ_S/ρ_0 is given[4,53] by the change in Helmholtz free energy arising from a superfluid velocity v. The defining relation for ρ_S^D/ρ_0 may be taken as,[45]

$$F_{\rm eff} = \frac{\hbar^2}{2m}\rho_S^D \int dx (\nabla\Phi)^2, \tag{13}$$

where Φ is the phase of the order in the liquid which explicitly includes phase twists over the length L. Prokof'ev and Svistunov[45] show that, from $F_{\rm eff}$, the probability of observing a number of phase twists J and winding number W are both Gaussian in J and W as obtained in Ref. 46 from H_{LL}. Specifically, the probability of observing a W obtained from $F_{\rm eff}$ is[45]

$$P^D(W) \propto \exp\left(-\frac{1}{2}\frac{LT}{\sigma\rho_S^D}W^2\right) = \exp\left(-\frac{1}{2}\alpha^D W^2\right) \tag{14}$$

in 1D. Eq. (14) is the same as the LL $P(W)$ in Eq. (9) with α replaced by α^D where

$$\alpha^D = \alpha_0\left(\frac{\rho_S^D}{\rho_0}\right)^{-1}. \tag{15}$$

From the general relation $\rho_S/\rho_0 = \alpha_0\langle W^2\rangle$ and using $P^D(W)$ in Eq. (14) to evaluate $\langle W^2\rangle$ we obtain Eq. (6) with α replaced by α_D, i.e.

$$\rho_S/\rho_0 = \left(\frac{\alpha_0}{4}\right)\frac{|\Theta_3''(0, e^{-\alpha^D/2})|}{\Theta_3(0, e^{-\alpha^D/2})} \tag{16}$$

This provides a relation[45,54] between ρ_S/ρ_0 and ρ_S^D/ρ_0.

In a uniform system (Galilean invariant), if LL predictions are correct, we expect $P(W)$ in Eq. (9) to be correct with $v_J = v_J^0$ and $\alpha = \alpha_0$. Comparing Eqs. (9) and (8) with Eqs. (15) and (14) requires $\rho_S^D/\rho_0 = 1$ for a uniform system. In disorder or in a periodic external potential, v_J can differ from v_J^0. However, if the LL predictions hold with v_J a constant, then we expect ρ_S^D/ρ_0 to be a constant independent of T or L, i.e. $\rho_S^D/\rho_0 = v_J/v_J^0$ to be constant. In disorder we can fit Eq. (16) to the PIMC ρ_S/ρ_0 and obtain ρ_S^D/ρ_0. Indeed Machta and Guyer[54] and Prokof'ev and Svistunov[45] have proposed this fit to obtain ρ_S^D/ρ_0. To do this, they propose a limit of Eq. (16) valid at large LT. The limit, is obtained by keeping only $W = \pm 1$ in the numerator and $W = 0$ in the denominator in Eq. (16) so that Eq. (16) reduces to,

$$\frac{\rho_S}{\rho_0} = \alpha_0 2\exp\left[-\frac{1}{2}\alpha_0\left(\frac{\rho_S^D}{\rho_0}\right)^{-1}\right]. \tag{17}$$

The full expression Eq. (16) or the limit Eq. (17) proposed in Refs. 45 and 54 can be fitted to the PIMC ρ_S/ρ_0 to determine ρ_S^D/ρ_0, as we do in the present paper.

III. MODEL OF THE NANOPORE AND METHODS

We simulate liquid ^{4}He confined in a nanopore described by the Hamiltonian,

$$\hat{H} = -\frac{\hbar^2}{2m}\sum_{i=1}^{N}\Delta_i + \sum_{i<j}^{N}U(r_{ij}) + \sum_{i=1}^{N}V(\rho_i), \tag{18}$$

where N is the number of ^{4}He atoms of mass m, $U(r)$ represents the interaction between ^{4}He atoms modeled by the Aziz potential[55] and $V(\rho)$ is the confining potential at a distance ρ from the center of the pore. To reduce the system size, we include the effect of the amorphous solid ^{4}He layers on the interior walls of the nanopore in the external potential $V(\rho)$. Our model is thus exactly the same as that used previously in Ref. 43.

The walls of real porous media plus solid ^{4}He layers are rough and irregular. This leads to a disordered confining potential for the liquid helium. In order to model the irregularity of the potential we have, as in Ref. 43, added fictitious fixed particles to the nanopores at random positions along the whole length of the pore and at all angles, separated from 2.5 Å to 3.5 Å from its axis. The average linear density of the fixed particles was 1 Å^{-1}. We represented their interaction with the helium atoms by a Lennard-Jones potential with parameters ϵ_d = 1.5 K and $\sigma_d = 2$ Å. The effect of this external potential is the creation of random pockets of stronger attraction or repulsion. For a given length, L, of the nanopore, the impurity potential is the same for all densities of the ^{4}He in the pore.

Finite temperature calculations are performed using the finite temperature worm algorithm path-integral Monte Carlo[6,56]. The values of the discretized imaginary time $\delta\tau$ were the same as in Ref. 43, i.e. 0.004 K^{-1}.

For calculations at zero temperature the second-order diffusion Monte Carlo method was used[57], which solves stochastically the Schrödinger equation written in imaginary time. The details of the method are given in Ref. 57 The guiding wave function was as usual constructed as $\Psi = \prod_{i<j} f(r_{ij})\phi(\rho_i)$, where $f(r) = \exp(-(b/r)^5)$ and $\phi(\rho)$ was the exact single-particle solution in the confining potential $V(\rho)$. Care was taken to eliminate any residual biases, such as the time-step or the population-size bias.

IV. RESULTS

A. Uniform nanopores

1. *Bulk liquid ^{4}He density*

Fig. 1 shows the superfluid fraction, ρ_S/ρ_0, the OBDM, $n(x)$, and the pair distribution function, $g(x)$, of 1D liquid ^{4}He confined in a uniform nanopore of radius

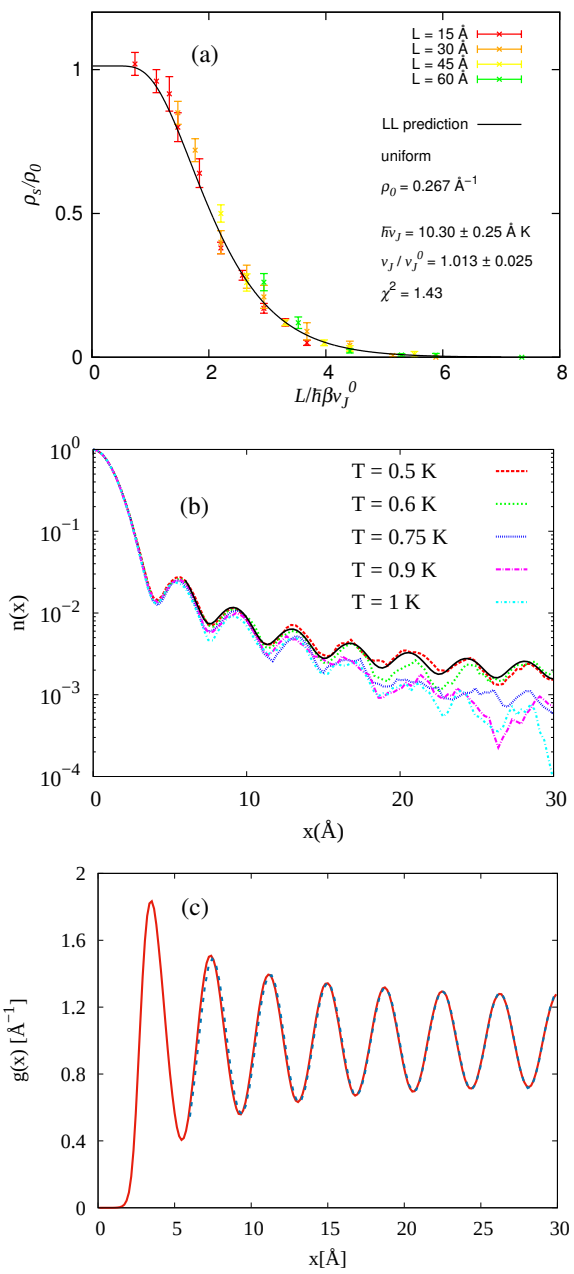

FIG. 1. (Color online) The (a) superfluid fraction, ρ_S/ρ_0, (b) one body density matrix, $n(x)$, and (c) pair distribution function, $g(x)$, of liquid ^{4}He confined in a uniform nanopore of radius $R = 3$ Å. The 3D liquid density in the pore, $\rho^{'} = 0.0212$ Å^{-3}, (linear density $\rho_0 = 0.267$ Å) is set close to the density of bulk liquid ^{4}He at SVP, $\rho = 0.0218$ Å^{-3}. The PIMC data for ρ_S/ρ_0 and $n(x)$ are from Ref. 43. The LL prediction for ρ_S/ρ_0 is fitted to the PIMC ρ_S/ρ with $\hbar v_J$ as a free fitting parameter. The error of the individual ρ_S/ρ_0 values is included in the fit. The fit is good with a χ^2 near unity. The best fit value of $\hbar v_J$ agrees with the uniform liquid, LL value, $\hbar v_J^0 = \pi(\hbar^2/m)\rho_0 = 10.17$ K Å, within the fit error. The PIMC $n(x)$ and the DMC $g(x)$ show long range oscillations as predicted by LL theory, oscillations that are unique to 1D fluids.

$R = 3$ Å at bulk liquid ^{4}He density. The corresponding linear density of the ^{4}He is $\rho_0 = 0.267$ Å^{-1}, interatomic spacing $a = \rho_0^{-1} = 3.75$ Å, along the nanopore. At $R = 3$ Å, it is energetically very difficult for two He atoms to exchange positions in the pore. In this sense it is a 1D system.

In Fig. 1a and 1b, ρ_S/ρ_0 and $n(x)$ calculated using PIMC are reproduced from Ref. 43. The solid line in Fig. 1a is a fit of the LL prediction for ρ_S/ρ_0, Eq. (6), with the LL parameter $\hbar v_J$ treated as a free fitting parameter. The best fit value of $\hbar v_J$ agrees with LL expression of a uniform system, $\hbar v_J^0 = \pi(\hbar^2/m)\rho_0 = 10.16$ Å K, within fit precision. The fit is good with a χ^2 close to unity. The PIMC ρ_S/ρ_0 clearly scales as the product LT as predicted for 1D by LL theory. In Fig. 1b, the solid line is a fit of the LL prediction, Eq. (4), to the PIMC $n(x)$. Only the first term in the series for $n(x)$ was retained with B_1 and K as free fitting parameters. The fit of the LL prediction to the PIMC $n(x)$ is clearly good.

In Fig. 1c, the dots show the fit of the LL prediction, Eq. (3), to $g(x)$ calculated using DMC. Again only the first term in the series was retained with A_1 and K treated as free fitting parameters. The fit is excellent and the K value obtained from the fit agrees well with K calculated from the equation of state and $S(q)$. The $g(x)$ clearly shows the long range oscillations characteristic of 1D at a linear density of $\rho_0 = 0.267$ Å^{-1}.

Eqs. (3) and (4) are valid for a LL liquid with periodic BCs over a length $L \to \infty$. For finite L, the $\rho_0 x$ in the denominators of the terms in Eqs. (3) and (4) should be replaced by $\rho_0 x \to \rho_0(L/\pi)|\sin(\pi x/L)|$ (see Eqs. (61) and (62) of Cazalilla[58]). We actually show the finite L expressions in Fig. 1 but the difference from Eqs. (3) and (4) is, except very near $L/2$, hardly perceptible on the scales shown in Figs. 1b and 1c.

2. *Density dependence*

We now explore the density dependence of 1D liquid ^{4}He. Fig. 2 shows the energy per particle, $e(\rho_0) = E(\rho_0)/N$, the pressure, $p(\rho_0)$, and the sound velocity, $v_S(\rho_0)$, of liquid ^{4}He in the uniform nanopore ($R = 3$ Å) versus the linear density, ρ_0. As the temperature is lowered the finite temperature PIMC results approach the T =0 K DMC values. $E(\rho_0)$/N has a broad minimum at $\rho_0 = 0.108$ Å^{-1}. Specifically, the pressure is zero at $\rho_0 = 0.108$ Å^{-1} showing that the equilibrium density in the nanopore is significantly lower than the linear density corresponding to bulk liquid ^{4}He, $\rho_0 = 0.267$ Å^{-1}. There is a modest pressure in the nanopores, $p \simeq 35$ bar, at $\rho_0 = 0.267$ Å^{-1}. The sound velocity goes to zero at $\rho_0 = 0.09$ Å^{-1} which defines the spinodal density where the 1D liquid is mechanically unstable. At the spinodal density, the uniform liquid appears to separate into linear droplets. The spinodal density lies very close to the equilibrium density.

Fig. 3 shows the Luttinger Liquid parameter K of

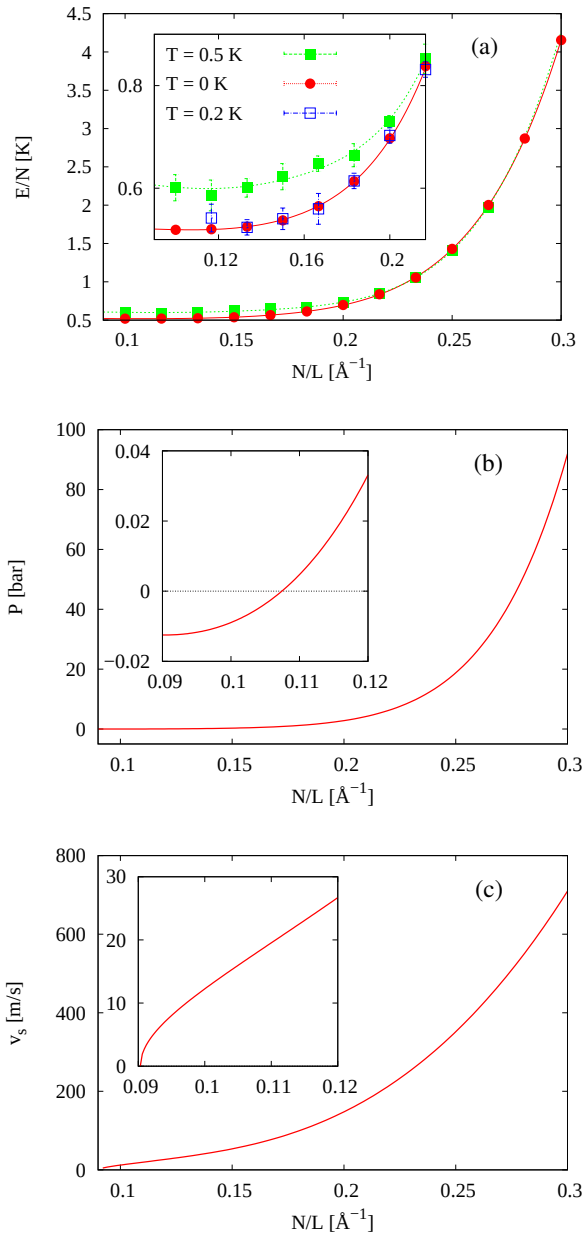

FIG. 2. (Color online) (a) The energy per Boson, $e(\rho_0)$, versus linear density, ρ_0, of 1D liquid ^{4}He in a nanopore of radius $R = 3$ Å. $e(\rho_0) = E(\rho_0)/N$ has a broad minimum at $\rho_0 \simeq 0.108$ Å^{-1}. (b) The pressure versus ρ_0. The pressure is zero at $\rho_0 = 0.108$ Å^{-1}. At ρ_0= 0.267 Å, the pressure is $P \simeq 35$ bar. (c) The sound velocity, v_S versus ρ_0. The LL parameter is $K = v_J^0/v_S$. The sound velocity vanishes at ρ_0= 0.09 Å^{-1}which defines the spinodal density where the 1D liquid becomes mechanically unstable to droplet formation.

the 1D liquid versus linear density ρ_0. The K calculated from the equation of state (the sound velocity), the static structure factor, $S(q)$, and from fits to the $g(x)$ agree well e.g. within a few percent at $\rho_0 = 0.25$ Å^{-1}. The K obtained from $g(x)$ is less well determined at lower densities since the amplitude of the oscillations in $g(x)$ is

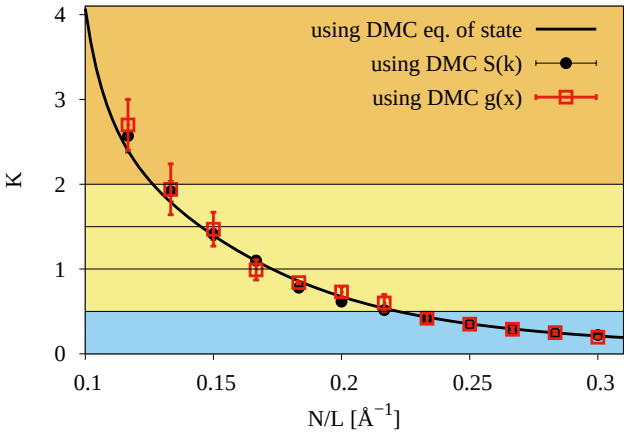

FIG. 3. (Color online) The Luttinger liquid parameter $K = (v_J^0/v_N)^{1/2}$ versus density $\rho_0 = N/L$ between $\rho_0 = 0.10$ Å^{-1} and $\rho_0 = 0.30$ Å^{-1}($\rho_0 = 0.090$ Å^{-1} is the spinodal density and $\rho_0 = 0.267$ Å^{-1}is the linear density corresponding to bulk liquid ^{4}He density at SVP). The solid line is K calculated from the equation of state. The solid circles and open squares are K calculated from the static structure factor, $S(q)$, and pair correlation function, $g(x)$, respectively. K varies from $K \gtrsim 2.0$ at the equilibrium density, $\rho_0 = 0.108$ Å^{-1}, to $K < 0.5$ at $\rho_0 = 0.267$ Å^{-1}.

smaller at lower densities and the linear region of $S(q)$ is reached only at low q. K varies from $K \geq 2$ at and below the equilibrium density $\rho_0 = 0.108$ Å^{-1} to $K < 0.5$ at $\rho_0 > 0.23$ Å^{-1}. Essentially at lower density, where the interaction is weaker, the kinetic energy (v_J) becomes relatively more important than the potential energy (v_N). $K = (v_J^0/v_N)^{1/2}$ is a sensitive function of linear density $\rho_0 = N/L$.

Fig. 4 shows the PIMC superfluid fraction, ρ_S/ρ_0, at four linear densities between $\rho_0 = 0.25$ Å^{-1} and $\rho_0 = 0.10$ Å^{-1}, the latter close to the spinodal density $\rho_0 = 0.09$ Å^{-1}. At the higher densities, $\rho_0 = 0.20$ Å^{-1} and $\rho_0 = 0.25$ Å^{-1}, the LL prediction fits the PIMC ρ_S/ρ_0 well, the χ^2 is close to unity and the best fit value of $\hbar v_J$ agrees with the uniform system value $\hbar v_J^0$, as in Fig. 1a. However, at lower density, $\rho_0 = 0.133$ Å^{-1} and $\rho_0 = 0.10$ Å^{-1}, the χ^2 is significantly larger. At lower density there does not appear to be a systematic deviation of the PIMC ρ_S/ρ_0 from the LL predictions. Rather there is a wider scatter of the PIMC ρ_S/ρ_0. The wider scatter may arise because at low density we have fewer atoms (lower statistics) in a given length L and L cannot be too long or there will be little or no winding. In addition, the density $\rho_0 = 0.10$ Å^{-1} is close to the spinodal density and in the PIMC simulations we observe periods of separation of the liquid into droplets during the simulation, in which case LL scaling is not expected.

Fig. 5 shows the OBDM, $n(x)$, calculated using PIMC methods at five linear densities between $\rho_0 = N/L = 0.117$ Å^{-1} and $\rho_0 = 0.25$ Å^{-1}. As in Fig. 1b, the

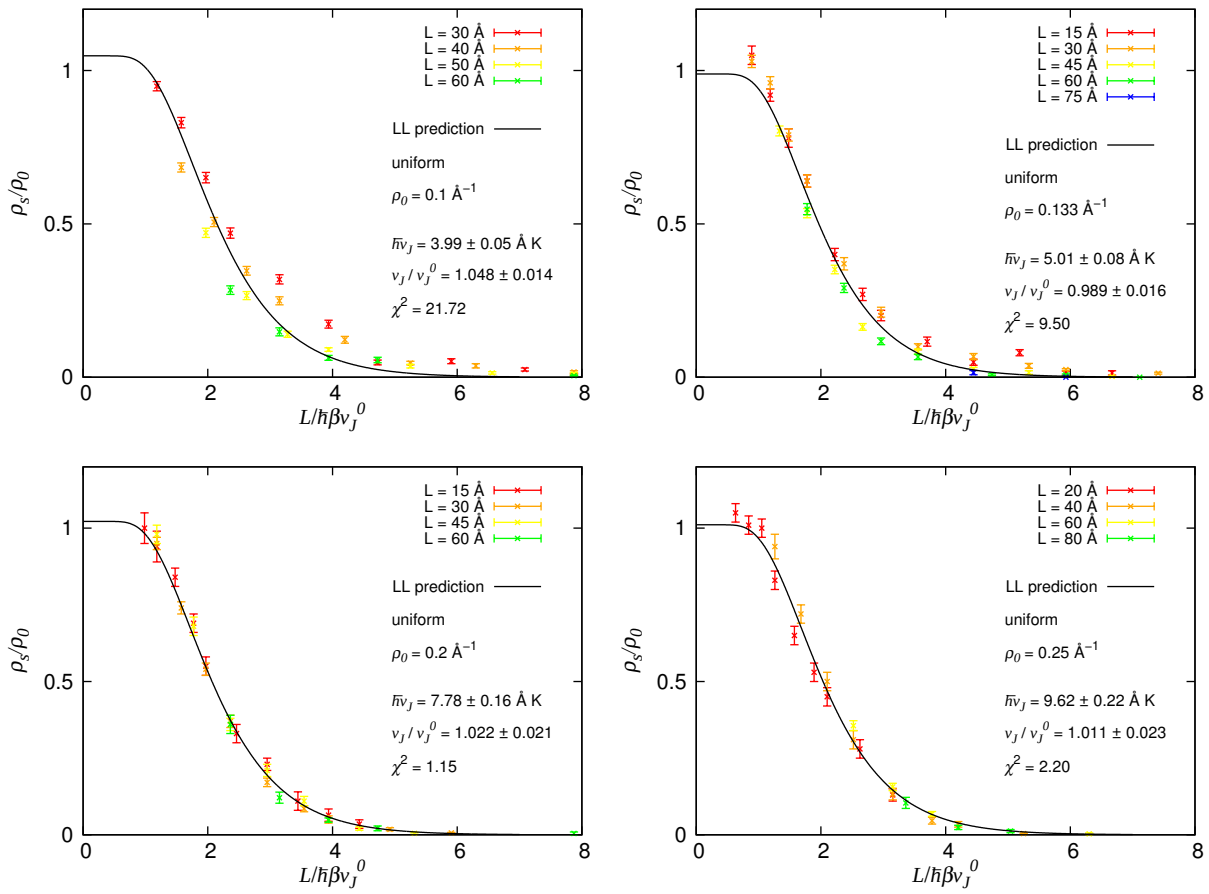

FIG. 4. (Color online) The PIMC superfluid fraction ρ_S/ρ_0 (data points) versus $L/\hbar\beta v_J^0 = (TL/\sigma\rho_0)/\pi \equiv \alpha_0/\pi$ (see Eq. (6)) of 1D liquid ^{4}He in a uniform nanopore (radius $R = 3$ Å) at four linear densities between $\rho_0 = 0.10$ Å^{-1} and 0.25 Å^{-1}. The LL prediction (solid line) fits well at all ρ_0 with LL parameter $\hbar v_J = \hbar v_J^0 = \pi(\hbar^2/m)\rho_0$, the uniform liquid value, within fit error.

$n(x)$ initially drops rapidly over a short distance x. This reflects the high localization of the atoms in real space (a wide momentum distribution) especially at higher density. The large amplitude oscillations in $n(x)$ at large x at $\rho_0 = 0.25$ Å^{-1} arise from the atomic correlations at high density. The fits to the PIMC OBDM shown (dotted lines) are Eq. (4) modified for the finite L periodic boundary conditions used in PIMC (see Eq. (62) of Ref. (58)). The LL parameter K obtained from the fit is consistent with K obtained from the equation of state and $S(q)$. The dashed-dotted line is Eq. (4) which shows that using the finite L expressions[58] makes little difference to the OBDM in this case.

Cazalilla[58] has derived expressions for correlation functions, $g(x)$ and $n(x)$, valid at finite temperature in the limit of infinite box size. These expressions show that the $T = 0$ K limit where the correlations functions show algebraic decay is reached only at lengths less than a thermal correlation length $L_T = \hbar v_s/(k_B T)$, i.e. at $x \le L_T$. At finite temperature and long lengths $x \ge L_T$, $g(x)$ and $n(x)$ cross over to exponential decay. At the three largest densities shown in Fig. 5, $L_T \gtrsim 30$ Å, so that finite temperature exponential scaling can not be observed for the $x \le 30$ Å shown. At $\rho_0 = 0.117$ Å^{-1}, $L_T \approx 9.4$ Å, and the heavy dotted line shows a fit of the finite temperature expression (Eq. (71) of Ref. (58)) to the PIMC OBDM. The finite T expression clearly fits the data well. We could not use the whole range up to half the box size, because the periodic boundary conditions cause the OBDM to have zero slope at half the box size, and in this particular case the slope started to change almost 10 Å before $L/2$. For the density 0.133 Å^{-1} no fit is provided because $L_T \approx 14$ Å so the range for both algebraic and exponential decay were too short.

The DMC pair distribution function versus linear density is shown in Fig. 6a for densities $0.1 \le \rho_0 \le 0.3$ Å^{-1}. While the amplitude of the oscillations decreases with decreasing density, there remain clearly observable oscillations at low density. The LL prediction for $g(x)$ fits the DMC $g(x)$ well down to the lowest densities.

Algebraic decay of $g(x)$ at $T = 0$ K is expected to cross over to exponential decay at finite temperature, as observed in $n(x)$. In $g(x)$ the cross over is most clearly observed in the decay of the oscillatons. Figure

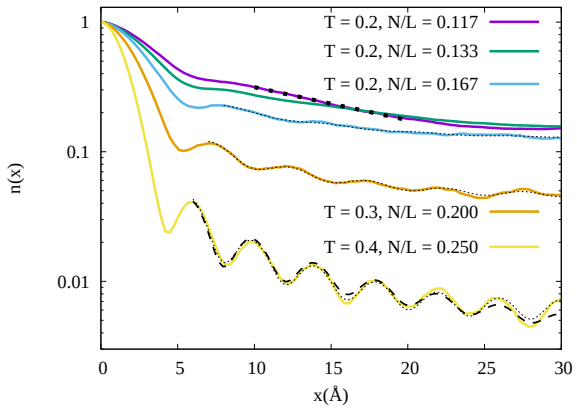

FIG. 5. (Color online) The PIMC OBDM, $n(x)$, at five linear densities between $N/L = \rho_0 = 0.117$ Å^{-1} and 0.25 Å^{-1}. The amplitude of the oscillations in $n(x)$ is larger at high density where the liquid has solid-like correlations. The dotted lines are fits of Eq. (4) modified to take account that the periodic BCs used have a finite L. Only the first term of these equations was retained with B_1 and K as adjustable parameters. The heavy dashed-dotted line at $N/L = 0.25$ Å^{-1} is a fit of Eq. (4), assuming $L \to \infty$ limit. Clearly, the approximation $L \to \infty$ introduces little error. The heavy dotted line at $N/L = 0.117$ Å^{-1} is a fit of the finite temperature $n(x)$ in a region of x where $n(x)$ shows exponential decay.

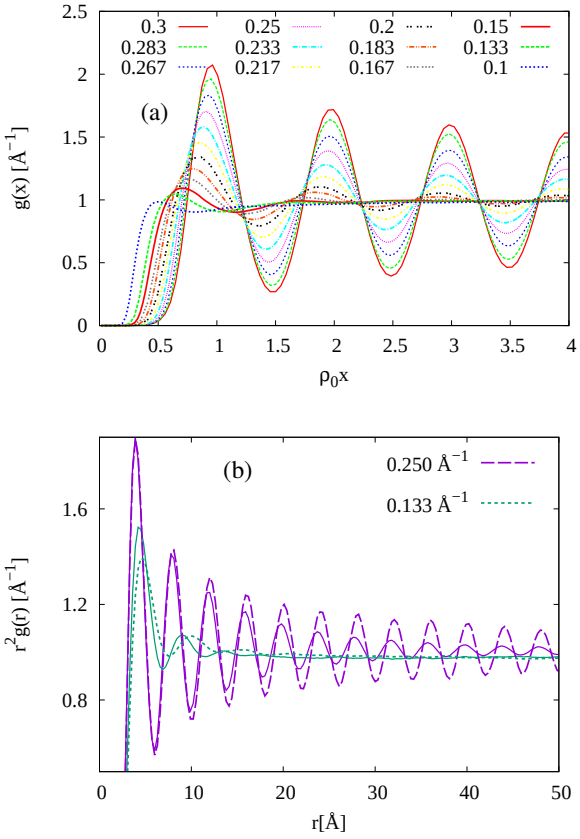

FIG. 6. (Color online) (a) The DMC pair distribution function, $g(x)$, at twelve linear densities ρ_0 (in Å^{-1}). The LL $g(x)$ fits well retaining the first term only in the series in Eq. (3) with A_1 and K as adjustable parameters As found for the OBDM, the amplitude of the oscillations in $g(x)$ increases with increasing density ρ_0. The LL parameter K obtained from $g(x)$ agrees well with K obtained from the equation of state and $S(q)$. (b) The PIMC pair distribution function at T=0.5 K (dashed lines) and T=1.5 K (full lines) at two linear densities. At sufficiently large x the correlation functions at finite T start to decay exponentially.

6b shows a zoomed pair distribution function at two temperatures. The more rapid decay at higher temperature is most clearly seen at the highest density shown, (0.250 Å^{-1}), where the thermal length $L_T \approx 54$ Å at 0.5 K and $L_T \approx 18$ Å at 1.5 K. The same type of behavior is present at all densities, but less visible.

Fig. 7 shows the static structure factor, $S(q) = \frac{1}{N}\langle\rho(q)\rho(-q)\rangle$, where $\rho(q)$ is Fourier transform of the density operator, $\rho(x) = \sum_l \delta(x - x_l)$ at T=0 K. $S(q)$ is shown for liquid ^{4}He in the nanopore at linear densities, $0.117 < \rho_0 < 0.30$ Å^{-1}. $S(q)$ is dominated by a single peak at $q = 2\pi\rho_0$. The peak height and sharpness of the peak increases with increasing density ρ_0. A small second peak emerges at $q = 4\pi\rho_0$ at the highest densities ρ_0. The dominant peak at $q = 2\pi\rho_0$ arises from the nearly solid like order in the 1D liquid and is characteristic of 1D. Using the relation,

$$\frac{1}{2\pi}\int dq e^{-iqx}[S(q) - 1] = \rho_0[g(x) - 1], \qquad (19)$$

we see that the dominant single peak in $S(q)$ at $q = 2\pi\rho_0$ will lead to oscillations in $g(x)$ dominated by a single term $A_1\cos(2\pi\rho_0 x)$. Thus the long range oscillations in $g(x)$ and sharp peak in $S(q)$ are complimentary characteristics of a highly correlated 1D fluid. Within precision we found that $S(q)$ was linear in q at $q \to 0$, although a low q value is needed to reach the linear region at low ρ_0. Using the relation, (10), we may see visually from Fig. 7 that the LL K decreases with increasing ρ_0.

B. Disordered nanopores

In the previous section we presented PIMC and DMC results for ρ_S/ρ_0, the OBDM, $n(x)$, the pair distribution function, $g(x)$, and $S(q)$ for liquid ^{4}He in a uniform nanopore of radius $R = 3$ Å. These properties were well described by LL expressions especially at higher linear density, $\rho_0 \geq 0.2$ Å^{-1}. In this section we present results for the 1D liquid in the nanopore containing disorder.

Fig. 8 shows ρ_S/ρ_0 for liquid ^{4}He at five linear densities in the nanopore containing point disorder in the walls as described in section III . The same disordered nanopore was used at all densities. The fits of the LL expression Eq. (6) to the PIMC ρ_S/ρ_0 are quite different from that of the uniform pore case. In disorder, the χ^2 is large even at high density $\rho_0 = 0.25$ Å^{-1} where χ^2 was small in the uniform case. Also, at $\rho_0 = 0.25$ Å^{-1} the

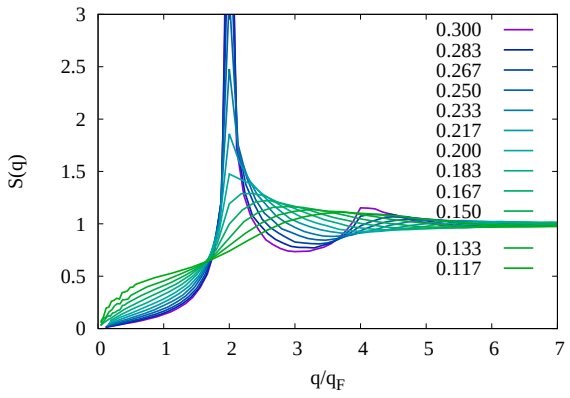

FIG. 7. (Color online) The DMC static structure factor $S(q)$ versus linear density $\rho_0 = a^{-1}$ in Å^{-1}. At larger ρ_0, $S(q)$ shows a peak at $q = 2\pi/a$. At the highest ρ_0, there is also a small peak at the second reciprocal lattice vector $q = 4\pi/a$. The LL parameter obtained from $S(q)$ agrees well with that obtained from $e(\rho_0)$ and $g(x)$.

three ρ_S/ρ_0 for the three different lengths L look somewhat different. There does not appear to be accurate scaling of ρ_S/ρ_0 with LT as in the uniform nanopore. At high density, the longer L appear to be associated with lower ρ_S/ρ_0, lower than predicted by Eq. (6).

If we interpret the PIMC ρ_S/ρ_0 in terms of the LL Hamiltonian, then the fit shown in Fig. 8 is a fit of Eq. (6) with v_J/v_J^0 in Eq. (8) as the fitting parameter. The best fit ratio v_J/v_J^0 is shown at each density in Fig. 8. Also, since from Eq. (6) $\rho_S/\rho_0 = v_J/v_J^0$ at $T = 0$ K, the value of v_J/v_J^0 can be read directly from ρ_S/ρ_0 at $T = 0$ K in Fig. 8. In disorder, LL theory predicts that ρ_S/ρ_0 should continue to scale with LT but with a constant $\hbar v_J$ that is different from $\hbar v_J^0$ and characteristic of the disorder. We note firstly that v_J/v_J^0 is not accurately determined. For example, the low values of v_J/v_J^0 at some densities in Fig. 8 appear to be associated with a lack of data at low LT where ρ_S/ρ_0 may go toward unity. Also as the homogeneous case, at the density $\rho = 0.1$ Å^{-1}, occasional separation into droplets in the course of the simulation is observed, which contributes to the low quality of the fit. Considering the remaining four densities, a value of $v_J/v_J^0 = 0.85 \pm 0.15$ independent of density could be proposed. At $\rho = 0.2$ Å^{-1}, the density for which we have most data, $v_J/v_J^0 = 0.95 \pm 0.01$ was obtained, however with the $\chi^2 \approx 50$. Excluding the data for the shortest length $L = 15$ Å, a $v_J/v_J^0 = 0.86 \pm 0.02$ would be obtained with $\chi^2 \approx 25$ at $\rho_0 = 0.2$ Å^{-1}.

The impact of disorder on ρ_S/ρ_0 is predicted[52] to be a sensitive function of K. In the present 1D ^{4}He, K depends on ρ_0 as shown in Fig. 3. For $K \geq 3/2$ 1D superfluidity is predicted to be robust in disorder. For $K \leq 3/2$ ($\rho_0 \gtrsim 0.14$ Å^{-1}) small amplitude disorder is predicted[52] to destroy 1D superfluidity. The suppression of ρ_S/ρ_0 at $K \leq 3/2$ is observed here only in the longer length samples investigated. At $\rho_0 = 0.2$ Å^{-1} and 0.25 Å^{-1} where $K < 3/2$ a small ρ_S/ρ_0 (near zero at $\rho_0 = 0.2$ Å^{-1}) is indicated at the longest L only. This suggests that ρ_S/ρ_0 can be suppressed to zero by disorder at $K \leq 3/2$ but a long sample is needed to reveal the suppression.

If we interpret the PIMC ρ_S/ρ_0 in Fig. 8 as an opportunity to determine the "dynamical" superfluid fraction ρ_S^D/ρ_0, then the fit in Fig. 8 is a fit of Eq. (16) with the "dynamical" ρ_S^D/ρ_0 in Eq. (15) as a free fitting parameter. The best fit values of ρ_S^D/ρ_0 are shown as $v_J/v_J^0 = \rho_S^D/\rho_0$ in Fig. 8 at each density. Clearly as quoted for v_J/v_J^0, all ρ_S^D/ρ_0 are less than one. Also from the fits ρ_S^D/ρ_0 is at least approximately independent of temperature over a temperature range of $0.2 \leq T \leq 2.5$ K. The ρ_S^D/ρ_0 are discussed further at the end of the Discussion.

Fig. 9 shows the impact of disorder on the OBDM, $n(x)$. The chief impact is a lowering of the height of the long range tail of $n(x)$ at $x \geq 5$ Å. The lowering of the height of the tail in $n(x)$ may be interpreted as a modest suppression of the superfluid order by disorder. This is consistent with the modest suppression of ρ_S/ρ_0 by disorder seen above. The oscillations in $n(x)$ with x at high density are little changed by disorder. Similarly, no oscillations in $n(x)$ are introduced by disorder at low density. Generally, the OBDM is less impacted by disorder than the ρ_S/ρ_0. Similarly, the pair correlation function, $g(x)$, shown in Fig. 10 is little modified by disorder.

V. DISCUSSION

In the previous section, we presented PIMC and DMC calculations of liquid helium confined to 1D in a narrow nanopore over a wide range of density. The Luttinger Liquid parameter varied from $K \geq 2$ to $K \leq 0.5$. Both uniform nanopores and nanopores containing disorder were investigated. The goal was to test how well a 1D liquid of ^{4}He atoms is described by LL theory.

A. Uniform 1D fluids

The ρ_S/ρ_0 of 1D liquid ^{4}He in a uniform nanopore was accurately described by LL theory. The LL expression, Eq. (7), fitted the PIMC ρ_S/ρ_0 well with $v_J = v_J^0$, the Galilean invariant liquid value at all densities and for all values of K considered. At very low densities, close to the spinodal density, the χ^2 of the fit was large compared to those at higher densities. This was attributed to the uniform fluid beginning to become unstable to 1D droplets close to the spinodal density.

The DMC $g(x)$ and $S(q)$ were well described by the $T = 0$ K LL predictions. At high density, $g(x)$ has long-range oscillations of wave vector $q = 2\pi\rho_0$ unique to 1D. The oscillations are characteristic of nearly solid order in the liquid at high density. The amplitude of the oscillations decreases with decreasing density, as the liquid becomes more gas like. The oscillations become unobservable near the equilibrium density ($p = 0$) which is close

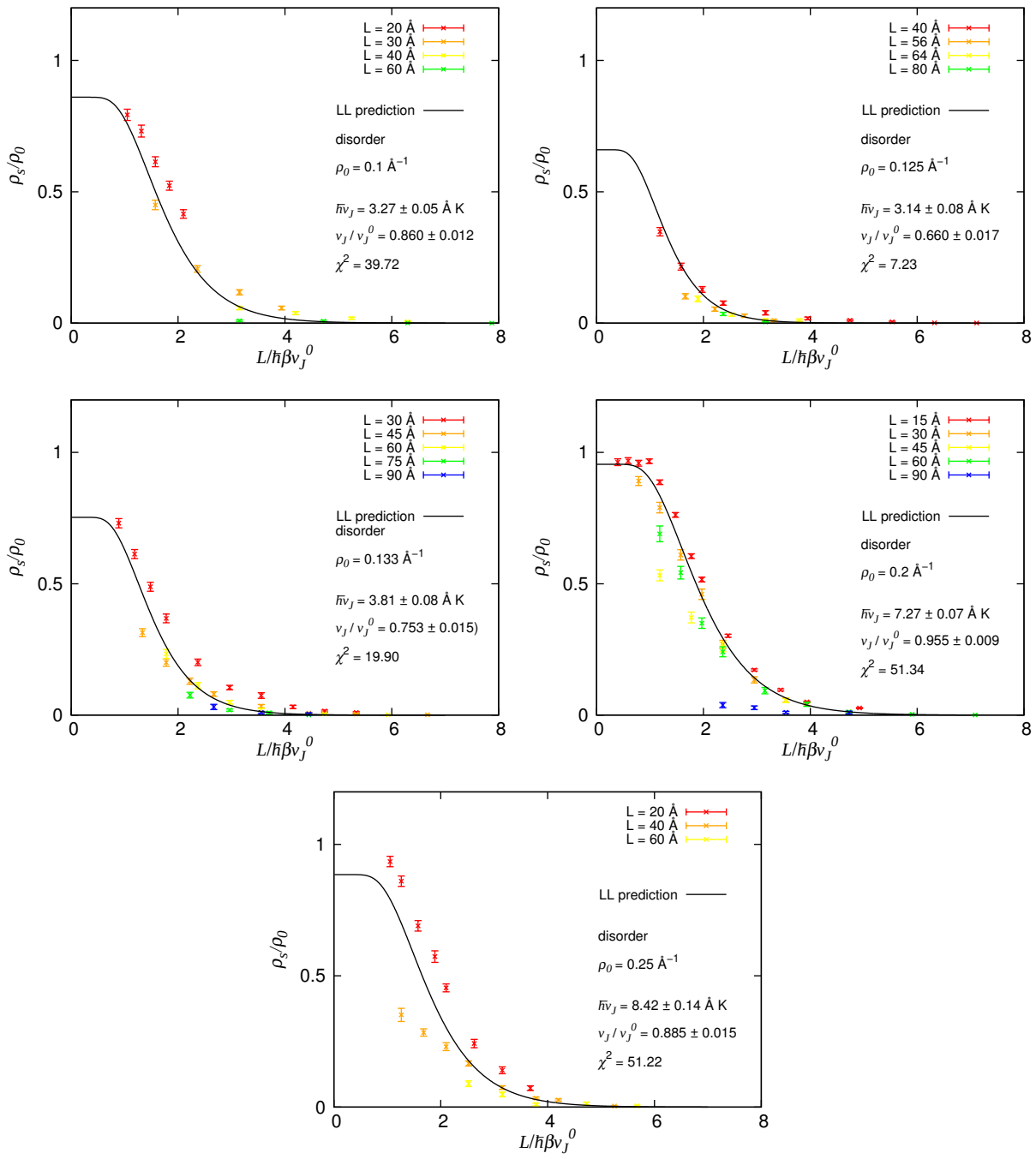

FIG. 8. (Color online) PIMC superfluid fraction, ρ_S/ρ_0, of 1D liquid ^{4}He (data points) in a nanopore (radius $R = 3$ Å) having disordered walls. Five linear densities ρ_0 between $\rho_0 = 0.10$ Å^{-1} and $\rho_0 = 0.25$ Å^{-1} with corresponding LL parameters $K > 2$ and $K < 0.5$ are shown. The solid line is the LL prediction fitted to the PIMC ρ_S/ρ_0 with $\hbar v_J$ a free fitting parameter. The fit is not good. The χ^2 is generally large, typically more than ten times the χ^2 found for the uniform case. The best fit $\hbar v_J$ differs from uniform liquid value $\hbar v_J^0$. When interpreted in terms of the dynamical superfluid fraction, ρ_S^D/ρ_0, defined by Machta and Guyer[54] and Prokof'ev and Svistunov[45] as discussed in the text, the ratio v_J/v_J^0 is interpreted as ρ_S^D/ρ_0.

to the spinodal density. The corresponding $S(q)$ has a large single peak at vector $q = 2\pi\rho_0$ at high densities, as expected for a $g(x)$ that oscillates. The PIMC OBDM, $n(x)$, equally shows oscillations in its long-range tail unique to 1D. Both the PIMC $g(x)$ and $n(x)$ were well fitted by the LL expressions, Eqs. (3) and (4), respectively for distances smaller than the thermal length. For high enough temperatures and long lengths, exponential decay of the correlation functions was observed. Near the spinodal density, $g(x)$ appeared to depend on

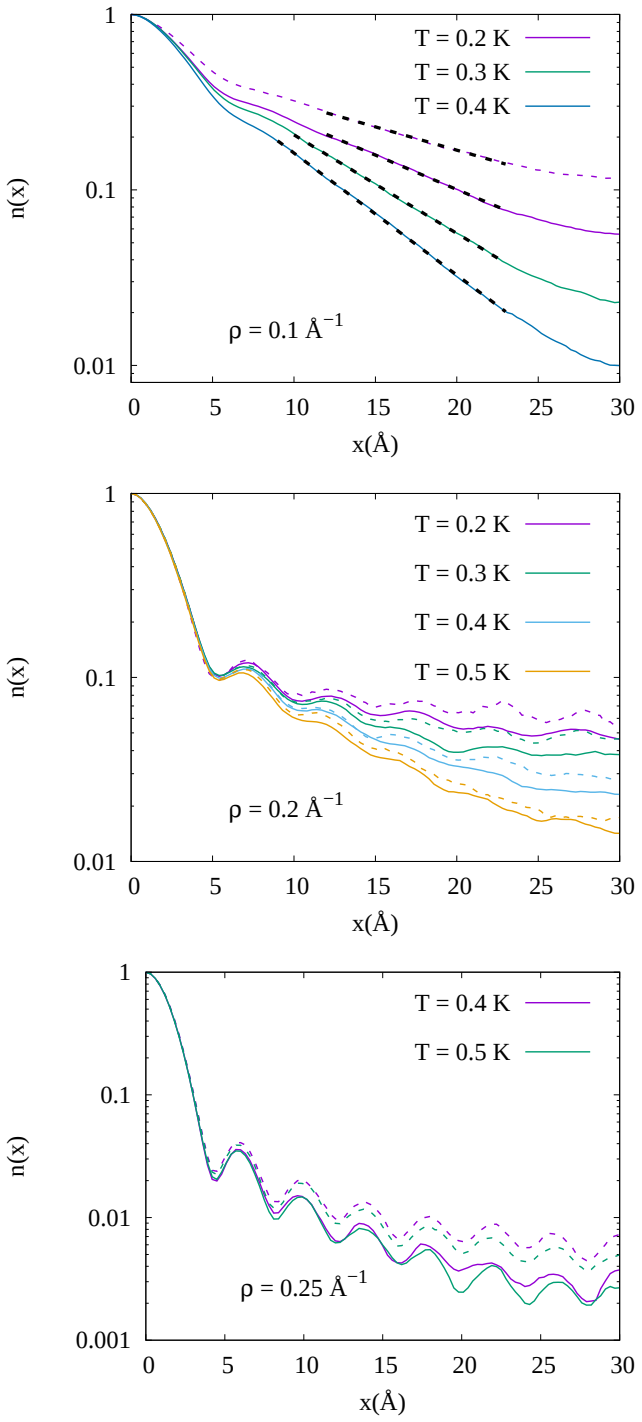

FIG. 9. (Color online) As Fig. 8 for the PIMC OBDM $n(x)$ at three densities ρ_0: solid lines in disorder, dashed lines in uniform pores. Disorder decreases the OBDM at longer x. In contrast to ρ_S/ρ_0, the LL prediction for $n(x)$, shown in Fig. 5, fits the PIMC OBDM in disorder quite well, especially at higher densities where the amplitude of the oscillations in $n(x)$ are observable. At $\rho_0 = 0.1$ Å^{-1}, the heavy dashed lines show a fit of the finite temperature $n(x)$ (e.g. Eq. (71) of Ref. (58)), $n(x) = \rho_0 B_0[(\pi/L_T)/\rho_0 \sinh(\pi x/L_T)]^{1/2K}$ where $L_T = \sigma\pi\rho_0/T$ ($\sigma = \hbar^2/mk_B$)) in the region of $x \gtrsim 2L_T$ where $n(x)$ decays exponentially with x. At shorter x, the finite T $n(x)$ reduces to the $T = 0$ K result, Eq. (4).

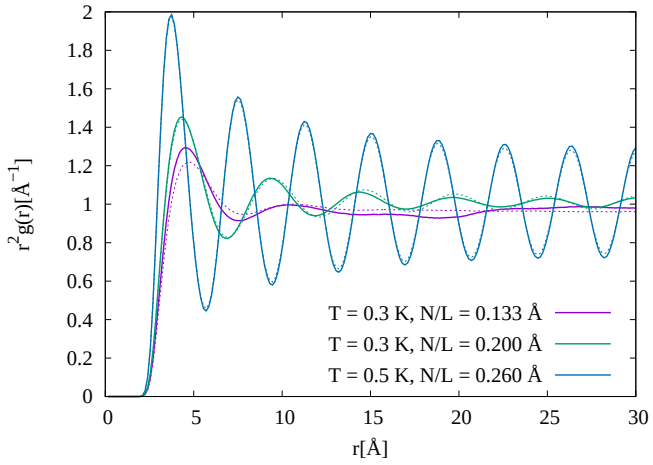

FIG. 10. (Color online) As Fig. 8 for the DMC pair distribution function $g(x)$.

temperature and to fall below unity, which is attributed to close proximity to droplet formation. There were no significant departures from LL predictions over the range of densities and K values investigated.

For a LL the height of the sharp peak in $S(q)$ at $q = 2q_F = 2\pi/a$ is predicted to scale with number of Bosons in the sample, N, as $S(2\pi/a) = AN^{1-2K}$. We tested this scaling at linear density $\rho_0 = 0.25$ Å^{-1}and found that $S(2\pi/a)$ does indeed scale as N^{1-2K} and the best fit $K = 0.344(14)$ obtained from the scaling agrees well with K calculated by other methods (see Fig. 3). The scaling suggests that in the thermodynamic limit the peak is infinite for $K < 1/2$. For density where $K > 1/2$ no increase of the main peak with the system size is observed, suggesting a finite value of the peak in the thermodynamic limit.

Liquid para-hydrogen (p-H_2) in 1D[48,49] or quasi-1D (e.g. at the center of carbon nanotubes or in harmonic potential confinement)[24,49–51,59] is similar to the present 1D ^{4}He liquid. The aim in confining p-H_2 in porous media is to suppress the freezing temperature of the liquid so that temperatures low enough to observe superfluidity might be reached. Recent reviews of this literature appear in Refs. 51 and 59. The aim of investigating 1D is to discover 1D superfluidity and to compare with LL theory. In these investigations, it is assumed that superflow in 1D liquid p-H_2 is possible if (and only if) the LL parameter K exceeds 3/2, a criterion predicted by LL theory.[52]

At high linear density, $S(q)$ of 1D liquid p-H_2 shows a large peak at $q = 2\pi\rho_0$ with corresponding large amplitude oscillations in $g(x)$ characteristic of solid-like atomic correlations, as found here for 1D liquid ^{4}He at high density. At high ρ_0, the LL parameter is small, $K \leq 0.5$. However, when the density is reduced K increases, as found here for 1D ^{4}He. A $K \geq 3/2$ at low density ($\rho_0 \lesssim 0.75$ Å^{-1}) has been reported[50]. However, for 1D and quasi 1D p-H_2, the spinodal density is reported[59,60]

at $\rho_0 = 0.20$ Å^{-1}. This means the low density where a $K \geq 3/2$ is reported[50] cannot be reached.

Near the equilibrium density[48,49,59], $\rho_0 = 0.22$ Å^{-1}($K \simeq 0.35$), the $S(q)$ and $g(x)$ of 1D p-H_2 are very similar to those found here for 1D ^{4}He at $\rho_0 = 0.22$ Å^{-1}. The two 1D liquids appear to be quite similar except that a much lower density can be reached in 1D liquid ^{4}He before the liquid becomes unstable. K always diverges at the spinodal density, but the density range over which K is large can be very small.

Bertaina *et al.*[61] have evaluated the LL parameter K and the dynamic structure factor of pure 1D ^{4}He. At high density, $\rho_0 > 0.2$ Å^{-1}, the K of pure 1D ^{4}He and ^{4}He in the present nanopore (Fig. 3) are the same. At lower density, K is somewhat lower for pure 1D ^{4}He since the spinodal density is lower in pure 1D ^{4}He ($\rho_{sp} = 0.026$ Å^{-1}).

Similarities can also be found between the present system and pure 1D ^{3}He[62] and spin-polarized hydrogen isotopes[63], especially at high densities in the quasi-solid regime where K <1/2. Due to hard-core interactions the energy and diagonal properties do not depend on the statistics but rather on the mass. At high linear densities the LL parameter K as a function of density is almost the same for all three hydrogen isotope systems.[63] ^{3}He enters[62] the K <1/2 regime at a linear density of 0.19 Å^{-1} which is quite close to the value obtained in this work. The difference arising from the mass becomes more apparent at lower density. In particular, neither of the 1D systems mentioned posesses a two-body bound state. Thus as the density is lowered the K parameter either increases up to 1 (for spin-polarized hydrogen) or shows a nonmonotonic behaviour, reaching a maximum higher than 1 and decreasing towards 1 as the density goes to zero. The height of the maximum increases in the vicinity of the two-body bound states.

B. 1D fluid in disorder

A 1D fluid in a disordered nanopore may also be well described by LL theory[10]. The present PIMC ρ_S/ρ_0 for 1D ^{4}He in disorder did not, however, obviously scale as LT. At higher densities definite departures from LT scaling appeared with a dependence on L evident. The fits of Eq. (6) to the PIMC ρ_S/ρ_0 in disorder also had a large χ^2, much larger than the χ^2 found for a uniform 1D liquid. The largest χ^2 were found at the highest densities. The fit suggested $v_J/v_J^0 = 0.85 \pm 0.15$ but with a large χ^2 , The general conclusion is that the LL expression describes the PIMC ρ_S/ρ_0 in disorder only approximately at best.

In the present model, disorder is introduced by adding impurities at random locations in the pore walls near the liquid. There can be a small variation in the magnitude of the disorder with periodic length L, an end effect. This variation with L would contribute to the departure of ρ_S/ρ_0 from LL scaling, i.e. to χ^2. We performed some exploratory calculations by creating disorder configurations at larger L as multiples of those from smaller ones, in particular L=60 Å as a multiple of L=30 Å or by using different random configurations. That had a very small effect on the quality of fits (χ^2 changed from 16 to 20) and thus could not account for the increase of the χ^2 from the homogeneous case, in particular for the highest densities, where the largest χ^2 were obtained. From the pair distribution function at lower densities and creation of faint aperiodic oscillations, it appears that particles are affected by the creation of random pockets of attraction and repulsion. The effect is larger for shorther lengths and may explain in part the increase of the χ^2 with respect to the homogeneous case. In summary, since large values of χ^2 were found at high ρ_0 and systematic departures from LL scaling at long L were obtained, we do not think the end effect makes a significant contribution to χ^2 and departures from LL character.

LL theory[52] also predicts 1D superfluidity to be fragile in disorder for $K \leq 3/2$, robust to disorder for $K \geq 3/2$. We found ρ_S/ρ_0 to be robust at $K \geq 3/2$. The fragility of ρ_S/ρ_0 in disorder at $K \leq 3/2$ was observed only in the long L samples. That is, at $\rho_0 \geq 0.2$ Å^{-1} where $K < 3/2$, ρ_S/ρ_0 was suppressed in disorder at long L only, e.g. at $\rho_S/\rho_0 = 0.2$ Å^{-1} and $L = 90$ Å, ρ_S/ρ_0 is nearly zero at all T investigated. Since the prediction draws on renormalization group methods, a long sample may be required to observe the cross over. Similarly, the OBDM was reduced by disorder more at long lengths (x) than at short lengths in Fig. 9.

At lower densities, where $K > 3/2$ and we expect the superfluidity to be robust, we have examined one additional, somewhat simpler model. Fixed fictitious particles of linear density 0.1 Å^{-1} were added randomly along the length and all angles, at a distance 2.5 Å from the axis. Half of the particles were interacting attractively, and half repulsively with the He atoms via the potential $\pm D/r^3$, with $D = 10$ K Å^3. The average of this additional interaction potential is zero, and its maximum within the space occupied by the helium atoms was less than 10% of the potential energy per particle. Although the values of the superfluid fraction were less suppressed below the uniform case, Luttinger liquid scaling with LT was not observed. Again, superfluidity was suppressed more at long lengths than would be expected from the suppression at shorter lengths.

The impact of disorder on superfluidity is predicted to depend on the strength of the disorder[38]. It is thus possible that by reducing D or ϵ_d one could recover the LL scaling in disorder. Our results, however, suggest, that LL scaling would be preserved only for very weak disorder. The additional difficulty with ^{4}He is the proximity to the spinodal decomposition, which prevents access to lower densities where K would be larger.

In an extensive study of hard core Bosons on a lattice with weak on site disorder, Doggen et al.[64] find a critical value of $K_c = 3/2$ in agreement with the predictions of Giamarchi and Schultz[52] (GS) . The disorder

is white noise in the sense that the disorder on nearest neighbor sites is uncorrelated. This agreement suggests that although the prediction of GS was derived using weak Gaussian correlated disorder the prediction may be valid for weak disorder more generally. For strong disorder, Doggen et al. find $K_c > 3/2$ and K_c is no longer constant. Rather K_c depends on the magnitude of the disorder. Again, our findings are limited. At low linear density, ρ_0, where $K > 3/2$ we find ρ_S/ρ_0 is not suppressed by disorder. However, at higher density $\rho_S/\rho_0 = 0.2$ Å^{-1}where $K = 0.7$ we find ρ_S/ρ_0 is suppressed to near zero for the long L samples consistent with GS predictions.

We may also interpret the PIMC ρ_S/ρ_0 as an opportunity to determine the dynamical ρ_S^D/ρ_0 proposed in Refs. 45 and 54. In this case, the fits to ρ_S/ρ_0 in Fig. 8 are interpreted as fits of Eq. (16) to the PIMC ρ_S/ρ_0 with ρ_S^D/ρ_0 in Eq. (15) as the fitting parameter. Before discussing the resulting ρ_S^D/ρ_0, we compare some expressions for ρ_S/ρ_0 in the literature.

1. Expressions for ρ_S/ρ

Using PIMC methods, we have calculated the "thermodynamic" superfluid fraction using the standard expression[53] Eq. (5), $\rho_S/\rho_0 = \alpha_0\langle W^2\rangle$. Specifically the mean square $\langle W^2\rangle$ was evaluated using PIMC.

If the LL Hamiltonian, Eq. (1), describes the 1D liquid, then the probability of observing a winding number W is given by Eq. (9) and the "thermodynamic" ρ_S/ρ is given by Eq. (7). In a disordered liquid v_J can differ from v_J^0 and in principle, depending on the fluid and disorder, $v_J > v_J^0$ is not excluded. The $T = 0$ K limit of Eq. (7) is v_J/v_J^0. If $v_J/v_J^0 > 1$, the LL Eq. (7) appears to permit the unphysical result $\rho_S/\rho_0 > 1$. In the present paper, Eq. (7) was fitted to the PIMC ρ_S/ρ which is always less than unity. Thus we found $v_J/v_J^0 = \rho_S^D/\rho_S \leq 1$.

DelMaestro and Affleck[46] have derived an expression for ρ_S/ρ_0 within LL theory,

$$\frac{\rho_S}{\rho_0} = 1 - \frac{4\pi^2}{\alpha}\langle J^2\rangle. \tag{20}$$

where $\alpha = \alpha_0(v_J/v_J^0)^{-1}$, $\alpha_0 = (TL/\sigma\rho_0)$ as before. If the LL Hamiltonian, Eq. (1), describes the liquid, the probability of observing a number J of phase twists across the liquid of length L is[46] $P(J) \propto e^{-(2\pi^2/\alpha)J^2}$. Since $\langle J^2\rangle \to 0$ as $T \to 0$, Eq. (20) gives $\rho_S/\rho_0 \to 1$ at $T = 0$ K. Eqs. (6) and (20) are similar except Eq. (6) gives $\rho_S/\rho_0 \to v_J/v_J^0$ at $T = 0$ K, Eq. (20) $\rho_S/\rho_0 \to 1$. The two expressions are identical for $v_J = v_J^0$. In earlier publications[20,22,43], Eq. (20) was fitted to PIMC values of ρ_S/ρ_0.

Prokof'ev and Svistunov[45] have derived an expression for ρ_S/ρ_0 in terms of the "dynamical" superfluid fraction ρ_S^D/ρ_0 introduced in section II ,

$$\frac{\rho_S}{\rho_0} = \frac{\rho_S^D}{\rho_0}\left[1 - \frac{4\pi^2}{\alpha^D}\langle J^2\rangle\right], \tag{21}$$

where $\alpha^D = \alpha_0(\rho_S^D/\rho_0)^{-1}$ as in Eq. (15). Eqs. (16) and (21) are identical. Specifically, the $T = 0$ limits of Eqs. (16) and (21) are $\rho_S/\rho_0 = \rho_S^D/\rho_0$. Although the physical meaning of Eq. (16) and (21) is very different from that of Eq. (6), the equations are identical with ρ_S^D/ρ_0 playing the role of v_J/v_J^0. Also, from Eq. (21) we see clearly that since PIMC values of ρ_S/ρ_0 satisfy $\rho_S/\rho_0 \leq 1$, a fit of Eq. (16) or Eq. (21) to PIMC ρ_S/ρ_0 will always give $\rho_S^D/\rho_0 \leq 1$.

2. Dynamical superfluid fraction

From Eq. (21), we see clearly that the "dynamical" ρ_S^D/ρ_0 and the "thermodynamic" ρ_S/ρ_0 are the same at $T = 0$ K. The central question is then, what is the temperature dependence of ρ_S^D/ρ_0? For a uniform (Galilean invariant) 1D liquid that is well described by the LL Hamiltonian with $v_J = v_J^0$, given the identity of Eqs. (7) and (16), we have $\rho_S^D/\rho_0 = 1$ for a uniform 1D liquid at all temperatures. Similarly, for a 1D liquid in disorder, given the fits shown in Fig. 8, there is no apparent temperature dependence in ρ_S^D/ρ_0 needed to get a reasonable fit of Eq. (16) to the PIMC ρ_S/ρ. For example, at $\rho_0 = 0.2$ Å^{-1} the fit is made over a range of LT values given by $0.5 < (L/\hbar\beta v_J^0) < 5$, where $L/\hbar\beta v_J^0 = (LT/\pi\sigma\rho_0)$. It is difficult to translate this into a definite temperature range, but a range $0 < T < 2.5$ K was used in calculations. This suggests a ρ_S^D/ρ_0 roughly independent of T up to $T \simeq 2$ K. A $\rho_S^D/\rho_0 \simeq 0.85 \pm 0.15$ independent of temperature is suggested at the considered densities.

The "dynamical" ρ_S^D/ρ_0 has been evaluated for atomic gases in a periodic external potential[27]. Both ρ_S^D/ρ_0 and ρ_S/ρ_0 are found to go from unity to zero as the density goes from incommensurate to commensurate, a superfluid to Mott insulator transition.

C. Comparison with experiment

The thermodynamic ρ_S/ρ given by Eq. (5) and evaluated using PIMC has been enormously successful in reproducing the observed ρ_S/ρ in 2D and 3D fluids[4,6,53,65]. It is tempting to compare the present model and thermodynamic ρ_S/ρ and OBDM with measurements of liquid ^{4}He in fully filled nanopores[14,15,66] of diameter 28 Å and 47 Å. However, the ρ_S/ρ observed in these nanopores has a transition temperature (e.g. $T_c = 0.9$ K for d = 28 Å) characteristic of 2D or 3D. In contrast, the ρ_S/ρ_0 in 1D has no thermal T_c. The temperature dependence of ρ_S/ρ in nanopores[14] below T_c is also quite different from that of ρ_S/ρ_0 in 1D. In nanopores, the phase at temperatures above T_c is a Bose glass (BG) phase[18,19,67,68]. The

BG phase supports well defined phonon modes in puddles of BEC separated by normal fluid[66,68,69]. The interpretation of the BG phase in terms of puddles of BEC has recently been made in Bose gases in traps[70].

Rather than 1D like, the observed ρ_S/ρ in nanopores[14] looks 2D like with a T_c. In nanopores of diameter 28 Å (liquid pore radius $R \simeq 9$ Å), the liquid ^{4}He is deposited predominantly in 2D layers[20,43]. A PIMC calculation of ρ_S/ρ and the OBDM, $n(x)$, of ^{4}He in the liquid layers[43] shows that both ρ_S/ρ_0 and $n(x)$ are 2D like[43] with a $T_c = 1.4$ K, which is close to the $T_c = 0.9$ K observed in nanopores, $d = 28$ Å. Extensive measurements of ρ_S/ρ in films of ^{4}He in nanopores have also been made[11,13]. In interconnected gelsils, the superfluid-normal transition is readily interpreted[18,19,67,68,71] as a superfluid-BG transition in 3D.

VI. CONCLUSION

The present DMC and PIMC results show that homogeneous liquid ^{4}He confined to 1D in a uniform nanopore is well described by LL theory. When disorder is added to the same nanopore, the PIMC superfluid fraction, ρ_S/ρ_0, retains only roughly the shape expected for 1D. The ρ_S/ρ_0 does not scale well with LT and a fit of the LL expression has a large χ^2. In disorder the ρ_S/ρ_0 becomes length dependent and ρ_S/ρ_0 is suppressed to near zero by disorder at $K < 3/2$ only in the longer length samples. The long range part of the OBDM is reduced most by disorder. The dynamical superfluid fraction, ρ_S^D/ρ_0, is calculated in terms of the thermodynamic, PIMC ρ_S/ρ_0 in disorder. The two are the same at $T = 0$ K. Within precision we find ρ_S^D/ρ_0 is independent of temperature (e.g. up to 2 K in 1D liquid ^{4}He).

VII. ACKNOWLEDGEMENTS

The authors gratefully acknowledge Massimo Boninsegni for providing the PIMC code used in this work and for valuable discussions. They thank Ian Affleck, Adrian Del Maestro, and Marcus Holtzmann for valuable discussions and insights on reduced dimensional systems and phase transitions. HRG thanks the Theory Group, Institut Laue Langevin for hospitality where part of this paper was written. This work was supported by the U.S. DOE, Office of Basic Energy Sciences (BES), Grant No. DEFG02-03ER46038 and in part by the Croatian Science Foundation under the project number IP-2014-09-2452 and Croatian Ministry of Science and Education.

[1] S. N. Bose, Z. Phys. **26**, 178 (1924).
[2] A. Einstein, Sitzungsber. Kgl. Preuss. Akad. Wiss., Phys. Math. Kl. **261** (1924).
[3] F. London, *Superfluids*, vol. 2 (Wiley, New York, 1954).
[4] D. M. Ceperley, Rev. Mod. Phys. **67**, 279 (1995).
[5] O. Penrose and L. Onsager, Phys. Rev. **104**, 576 (1956).
[6] M. Boninsegni, N. Prokof'ev, and B. Svistunov, Phys. Rev. Lett. **96**, 070601 (2006).
[7] A. J. Leggett, *Quantum Liquids: Bose Condensation and Cooper Pairing in Condensed Matter Systems* (Oxford University Press, Oxford, 2006).
[8] J. M. Kosterlitz and D. J. Thouless, J. Phys. C: Solid State **6**, 1181 (1973).
[9] D. R. Nelson and J. M. Kosterlitz, Phys. Rev. Lett. **39**, 1201 (1977).
[10] F. D. M. Haldane, Phys. Rev. Lett. **47**, 1840 (1981).
[11] N. Wada, J. Taniguchi, H. Ikegami, S. Inagaki, and Y. Fukushima, Phys. Rev. Lett. **86**, 4322 (2001).
[12] N. Wada, Y. Minato, T. Matsushita, and M. Hieda, J Phys. Soc. Jap. **77**, 111012 (2008).
[13] N. Wada, Y. Minato, T. Matsushita, and M. Hieda, J. Low Temp. Phys. **162**, 549 (2011).
[14] J. Taniguchi, Y. Aoki, and M. Suzuki, Phys. Rev. B **82**, 104509 (2010).
[15] J. Taniguchi, R. Fujii, and M. Suzuki, Phys. Rev. B **84**, 134511 (2011).
[16] J. Taniguchi, K. Demura, and M. Suzuki, Phys. Rev. B **88**, 014502 (2013).
[17] T. Eggel, M. A. Cazalilla, and M. Oshikawa, Phys. Rev. Lett. **107**, 275302 (2011).
[18] K. Yamamoto, H. Nakashima, Y. Shibayama, and K. Shirahama, Phys. Rev. Lett. **93**, 075302 (2004).
[19] K. Yamamoto, Y. Shibayama, and K. Shirahama, Phys. Rev. Lett. **100**, 195301 (2008).
[20] A. Del Maestro, M. Boninsegni, and I. Affleck, Phys. Rev. Lett. **106**, 105303 (2011).
[21] A. Del Maestro, Int. J. Mod. Phys. B **26**, 1244002 (2012).
[22] B. Kulchytskyy, G. Gervais, and A. Del Maestro, Phys. Rev. B **88**, 064512 (2013).
[23] M. Boninsegni, A. B. Kuklov, L. Pollet, N. V. Prokof'ev, B. V. Svistunov, and M. Troyer, Phys. Rev. Lett. **99**, 035301 (2007).
[24] M. C. Gordillo and J. Boronat, Journal of Low Temperature Physics **157**, 296 (2009), ISSN 1573-7357.
[25] D. Jaksch, C. Bruder, J. I. Cirac, C. W. Gardiner, and P. Zoller, Phys. Rev. Lett. **81**, 3108 (1998).
[26] M. Greiner, O. Mandel, T. Esslinger, T. W. Hansch, and I. Bloch, Nature (London) **415**, 39 (2002).
[27] G. Boéris, L. Gori, M. D. Hoogerland, A. Kumar, E. Lucioni, L. Tanzi, M. Inguscio, T. Giamarchi, C. D'Errico, G. Carleo, G. Modugno, and L. Sanchez-Palencia, Phys. Rev. A **93**, 011601 (2016).
[28] T. Stöferle, H. Moritz, C. Schori, M. Köhl, and T. Esslinger, Phys. Rev. Lett. **92**, 130403 (2004).
[29] B. Gadway, D. Pertot, J. Reeves, M. Vogt, and D. Schneble, Phys. Rev. Lett. **107**, 145306 (2011).
[30] L. Tanzi, E. Lucioni, S. Chaudhuri, L. Gori, A. Kumar, C. D'Errico, M. Inguscio, and G. Modugno, Phys. Rev. Lett. **111**, 115301 (2013).
[31] L. Gori, T. Barthel, A. Kumar, E. Lucioni, L. Tanzi, M. Inguscio, G. Modugno, T. Giamarchi, C. D'Errico, and

G. Roux, Phys. Rev. A **93**, 033650 (2016).
[32] V. P. Michal, I. L. Aleiner, B. L. Altshuler, and G. V. Shlyapnikov, Proc. Natl. Acad. Sci. USA **113**, E4455 (2016).
[33] J. Mun, P. Medley, G. K. Campbell, L. G. Marcassa, D. E. Pritchard, and W. Ketterle, Phys. Rev. Lett. **99**, 150604 (2007).
[34] L. Tanzi, S. Scaffidi Abbate, F. Cataldini, L. Gori, E. Lucioni, M. Inguscio, G. Modugno, and C. DErrico, Scientific Reports **6**, 25965 (2016).
[35] K. Y. Arutyunov, D. S. Golubev, and A. D. Zaikin, Physics Reports **464**, 1 (2008).
[36] O. V. Astafiev, L. B. Ioffe, S. Kafanov, Y. A. Pashkin, K. Y. Arutyunov, D. Shahar, O. Cohen, and J. S. Tsai, Nature **484**, 355 (2012).
[37] Giamarchi, T., *Quantum Physics in One Dimension* (Oxford Univerrsity Press, Oxford, 2004).
[38] M. A. Cazalilla, R. Citro, T. Giamarchi, E. Orignac, and M. Rigol, Rev. Mod. Phys. **83**, 1405 (2011).
[39] A. Imambekov, T. L. Schmidt, and L. I. Glazman, Rev. Mod. Phys. **84**, 1253 (2012).
[40] K. Yamashita and D. S. Hirashima, Phys. Rev. B **79**, 014501 (2009).
[41] A. Kotani, K. Yamashita, and D. S. Hirashima, Phys. Rev. B **83**, 174515 (2011).
[42] I. Danshita, J. Low Temp. Physics **175**, 222 (2014).
[43] L. Vranješ Markić and H. R. Glyde, Phys. Rev. B **92**, 064510 (2015).
[44] J. Machta and R. A. Guyer, Phys. Rev. Lett. **60**, 2054 (1988).
[45] N. V. Prokof'ev and B. V. Svistunov, Phys. Rev. B **61**, 11282 (2000).
[46] A. Del Maestro and I. Affleck, Phys. Rev. B **82**, 060515 (2010).
[47] T. Volkoff, Y. Kwon, and K. B. Whaley, Phys. Rev. B **94**, 144510 (2016).
[48] M. Boninsegni, Phys. Rev. Lett. **111**, 235303 (2013).
[49] M. C. Gordillo and D. M. Ceperley, Phys. Rev. Lett. **85**, 4735 (2000).
[50] M. Rossi and F. Ancilotto, Phys. Rev. B **94**, 100502 (2016).
[51] T. Omiyinka and M. Boninsegni, Phys. Rev. B **93**, 104501 (2016).
[52] T. Giamarchi and H. J. Schulz, Phys. Rev. B **37**, 325 (1988).
[53] E. L. Pollock and D. M. Ceperley, Phys. Rev. B **36**, 8343 (1987).
[54] J. Machta and R. A. Guyer, J. Low Temp. Physics **74**, 231 (1989), ISSN 1573-7357.
[55] R. A. Aziz, F. R. W. McCourt, and C. C. K. Wong, Mol. Phys. **61**, 1487 (1987).
[56] M. Boninsegni, N. V. Prokof'ev, and B. V. Svistunov, Phys. Rev. E **74**, 036701 (2006).
[57] J. Boronat and J. Casulleras, Phys. Rev. B **49**, 8920 (1994).
[58] M. A. Cazalilla, J. Phy. B: Mol. Opt. Phys. **37**, S1 (2004).
[59] G. Ferré, M. C. Gordillo, and J. Boronat, Phys. Rev. B **95**, 064502 (2017).
[60] A. Del Maestro and M. Boninsegni, Phys. Rev. B **95**, 054517 (2017).
[61] G. Bertaina, M. Motta, M. Rossi, E. Vitali, and D. E. Galli, Phys. Rev. Lett. **116**, 135302 (2016).
[62] G. E. Astrakharchik and J. Boronat, Phys. Rev. B **90**, 235439 (2014).
[63] A. J. Vidal, G. E. Astrakharchik, L. V. Marki, and J. Boronat, New Journal of Physics **18**, 055013 (2016).
[64] E. V. H. Doggen, G. lemarié, S. Capponi, and N. Laflorencie, arXiv:1704.02257v2 1 (2017).
[65] D. M. Ceperley and E. L. Pollock, Phys. Rev. B **39**, 2084 (1989).
[66] S. O. Diallo, R. T. Azuah, D. L. Abernathy, J. Taniguchi, M. Suzuki, J. Bossy, N. Mulders, and H. R. Glyde, Phys. Rev. Lett. **113**, 215302 (2014).
[67] H. R. Glyde, O. Plantevin, B. Fak, G. Coddens, P. S. Danielson, and H. Schober, Phys. Rev. Lett. **84**, 2646 (2000).
[68] O. Plantevin, B. Fåk, H. R. Glyde, N. Mulders, J. Bossy, G. Coddens, and H. Schober, Phys. Rev. B **63**, 224508 (2001).
[69] J. Bossy, J. Ollivier, H. Schober, and H. R. Glyde, Euro. Phys. Lett. **98**, 56008 (2012).
[70] C. Meldgin, U. Ray, P. Russ, D. Chen, D. M. Ceperley, and B. Demarco, Nature Phys. **12**, 646 (2016).
[71] J. Bossy, J. V. Pearce, H. Schober, and H. R. Glyde, Phys. Rev. Lett. **101**, 025301 (2008).